

UNIVERSITY OF SCIENCE AND TECHNOLOGY OF HA NOI



INTERNSHIP REPORT

**A STUDY OF THE SIX MAJOR SOLAR FLARES RECENTLY
DETECTED FROM HA NOI AND LEARMONTH AT 1415 MHz
COMPARED WITH OTHER FREQUENCIES**

**SUPERVISORS : Professor Pierre Darriulat,
Dr. Nguyen Thi Thao**

STUDENT : Bui Van Tuan

DEPARTMENT : Space and Applications

INTAKE : 2013

ACADEMIC YEAR: 2014

LABORATORY : Vietnam Astrophysics Training Laboratory

Ha Noi – August, 2014

OUTLINES

I. INTRODUCTION TO VATLY.....	3
II. REPORT	3
1. THE SUN.....	3
<i>1.1 General properties.....</i>	<i>3</i>
<i>1.2 Structure of the Sun</i>	<i>4</i>
1.2.1 The core.....	5
1.2.2 Radiative zone.....	5
1.2.3 Convective zone.....	6
1.2.4 Photosphere.....	6
1.2.5 Atmosphere.....	7
<i>1.3 Magnetic field.....</i>	<i>8</i>
1.3.1 General features	8
1.3.2 Solar flares	9
1.3.3 Interplanetary field.....	9
1.3.4 Solar spots and solar cycle.....	10
1.3.5 Anomalies	11
<i>1.4 Evolution.....</i>	<i>12</i>
1.4.1 Birth of the Sun.....	12
1.4.2 Present phase.....	12
1.4.3 Death of the Sun.....	13
2. DATA REDUCTION.....	14
3. DETAILED STUDY OF THE SELECTED FLARES.....	20
<i>3.1 Learmonth-Ha Noi comparison at 1.4 GHz</i>	<i>20</i>
<i>3.2 Learmonth radio data at different frequencies.....</i>	<i>20</i>
<i>3.3 Other wavelengths.....</i>	<i>24</i>
4. CONCLUSION.....	26

I. INTRODUCTION TO VATLY

VATLY stands for Vietnam Astrophysics Training Laboratory. Its aim is to establish in Hanoi a team of researchers of international stature having the ambition to promote in the country teaching and research in fundamental sciences, and in particular in astrophysics. It was installed in the premises of the Institute for Nuclear Sciences and Technologies (INST) in 2001 in Hanoi.

It used to be associated with the Pierre Auger Observatory, in Argentina, that studies cosmic rays at extreme energies since the beginning until the early 2010s. The strong support that it received from the international Pierre Auger Collaboration was invaluable. Starting in 2010 research interests switched to radio astronomy. Much of it is made in collaboration with other institutes: With IRAP (Toulouse) using data collected at the Plateau de Bure Interferometer Array (PdBI) on the host galaxy of a remote ($z=2.8$) quasar gravitationally lensed by a galaxy in the foreground; with LERMA (Paris) using data collected at PdBI and Pico Veleta on CO and at Nançay and the Very Large Array on HI to observe the circumstellar shells of AGB stars and study the mass loss mechanism. In addition, it also does research at home using a 2.6 m diameter radio telescope on the roof of the laboratory tuned in the region of the 21 cm HI line, from which the data of the present work have been collected.

In addition to training master and PhD students, it welcomes for a few months internship master students and undergraduate students.

II. REPORT

The present report relates work done in VATLY in summer 2014 in the context of a two month internship, in collaboration with my classmate Nguyen Hoang Phuong Thanh.

Chapter 1 collects material that was given by our supervisor for us to study, mostly lecture notes and encyclopaedia articles. During our stay in VATLY, each of us was asked to give a presentation of part of this material, Thanh on solar flares and I on the general properties of the Sun. Chapter 2 describes the reduction of the data on which Thanh and I worked together. The third chapter describes work which I did alone (Thanh was working on another subject).

1. THE SUN

1.1 General properties

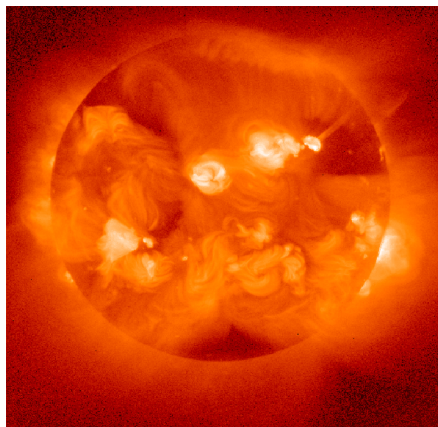


Figure 1.1 A radio picture of the Sun

The Sun, at the centre of the solar system, was born some five billion years ago from the gravitational collapse of a molecular cloud. It is located at 8.3 light-minutes (one astronomic

unit by definition) from the Earth. It is a star of the Main Sequence with a surface temperature of $\sim 5.8\text{kK}$.

The Sun produces its energy by fusing protons into alpha particles. There are more than 10^{11} other stars in that state in the Milky Way. It consists of hydrogen ($\sim 74\%$ in mass), helium ($\sim 24\%$ in mass), and traces of other elements. Its spectrum displays lines of metallic atoms, ionised or neutral, and a few hydrogen line of weak intensity. The solar corona dilutes continuously at high temperature into space, producing the solar wind, a supersonic flux of charged particles that reaches a few hundred astronomic units (AU) away. It is in motion on a circular orbit around the centre of the Milky Way at a radius of some 25'000 light years at a speed of 250 km/s toward Cygnus (a full revolution takes 250 million years). The Sun will keep burning its hydrogen for another five billion years, after what it will become a Red Giant before its core collapse into a White Dwarf and its envelope fade away as a Planetary Nebula.

1.2 Structure of the Sun

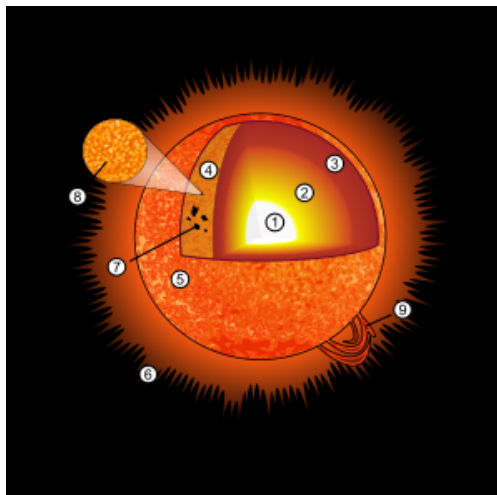


Figure 1.2. Structure of the Sun: 1. Core; 2. Radiative zone; 3. Convection zone; 4. Photosphere; 5. Chromosphere; 6. Corona; 7. Solar spots; 8. Granules; 9. Flares

The Sun is a yellow star of the Main Sequence making up some 99.86% of the total mass of the solar system. It is shaped as a nearly perfect sphere. It is made of plasma and rotates faster at the equator than at the poles. Rotation periods are 25.6 days at the equator and 33.5 days at the poles. However, as earth itself turns around the Sun, the mean rotation period seen from Earth is 28 days.

The Sun is a Population I star, therefore rich in heavy elements. It is probably the shock wave of one (or several) supernova that triggered the collapse of the cloud from which it is born, as suggested by the abundance of heavy elements, such as gold and uranium, which are very rare in Population II stars.

The edge of the Sun is somewhat smeared, density decreases exponentially as a function of radius in the vicinity of the surface. But it has a well-defined internal structure. The Sun radius is defined as that of the photosphere, meaning the layer above which gases are too cold or too diluted to radiate an important amount of light: it is the inner edge of this layer that can be seen by the naked eye.

The Sun interior is not directly observable and the Sun itself is opaque to electromagnetic waves. However, in the same way as seismology tells us about the inner structure of Earth from the seismic waves associated with earthquakes, helioseismology uses infrasonic pressure waves that travel inside the Sun to observe and measure its internal structure. Computer models of the Sun have been developed and make it possible to extrapolate the information down to its centre.

1.2.1 The core

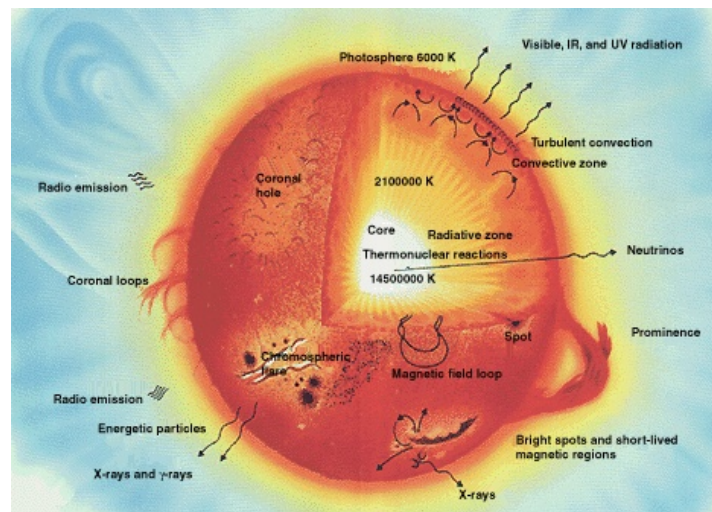


Figure 1.3 Schematic of the internal structure of the Sun

The core of the Sun reaches some 0.20 to 0.25 solar radii outward from the centre. It has a density of up to 150 g/cm^3 and a temperature nearing the millions of Kelvin (while the Sun surface temperature is only 5.8 kK). During most of the star life, it produces energy by nuclear fusion in a sequence of reactions converting hydrogen into helium, the so-called p-p cycle. Less than 2% of the energy is produced via the CNO cycle. Nuclear energy is produced in the core exclusively: the rest of the star is simply heated by the heat that flows from the core outward to the surface. Before being released in outer space, this energy is several times absorbed and reemitted during its journey inside the star.

Each second, some 10^{38} protons are converted into helium nuclei (out of the $\sim 10^{57}$ that the Sun contains). The mean power density is of the order of 0.2 mW/kg of matter, but the core power density is 150 times larger. As a comparison, the human body produces some 1.3 W/kg, namely 600 times more than the Sun. The core power density is relatively low: only 0.27 W/m^3 , namely much less than that of a candle. The nuclear fusion rate depends strongly on temperature and pressure, resulting in a stable equilibrium for the core: a small increase of the fusion rate increases the core temperature and makes it expand, thereby reducing the density and the fusion rate. Conversely a small decrease of the fusion rate induces a contraction and feeds back.

A few millimetres of solar plasma are sufficient to absorb the radiation produced by fusion, which is then reemitted isotropically at a slightly lower energy; the time it takes for the radiation produced in the core to reach the surface is very long, several tens of thousands years.

After having crossed the external convective layer, photons reach the external transparent layer and escape into space as visible light. A high energy photon produced in the core generates several millions of visible photons radiated this way. Fusion reactions produce also neutrinos that escape instantly because their interaction with matter is extremely weak.

1.2.2 Radiative zone

Between ~ 0.25 and ~ 0.7 solar radii, plasma is very hot and dense enough for the thermal radiation to transfer the produced heat outward. In this zone, although the temperature decreases with radius, (from 7 MK to some 2 MK), the temperature gradient is not sufficient for convection to play a significant role. Heat transfer is purely radiative – hydrogen and helium ions emit photons that are promptly absorbed before others be reemitted. Density drops by a factor 100 (from 20 g/cm^3 to only 0.2 g/cm^3) from the inner to the outer radiative zone.

Between the radiative and convective zones, there is an intermediate layer called tachocline. It is where one switches from a uniform rotation in the radiative zone to a differential rotation in the convective zone. Important shears result, successive layers sliding on top of each other. The fluid motion accelerates outward, producing magnetic field by dynamo effect.

1.2.3 Convective zone

In the external layer of the Sun, from 0.7 solar radii to the surface, plasma is no longer hot enough, nor dense enough, to transfer heat by radiation. It is the domain of convection, producing columns of heat exchange driving hot matter toward photosphere. As it reaches the surface, it cools down and dives again inward where it heats up when reaching the radiative zone. At the outer Sun radius, temperature has dropped to 5.7 kK and density to only 0.2 g/m^3 .

The thermal columns of the convective zone imprint a kind of granulation on the solar surface. The associated turbulences generate a local dynamo effect producing magnetic dipoles on the whole surface.

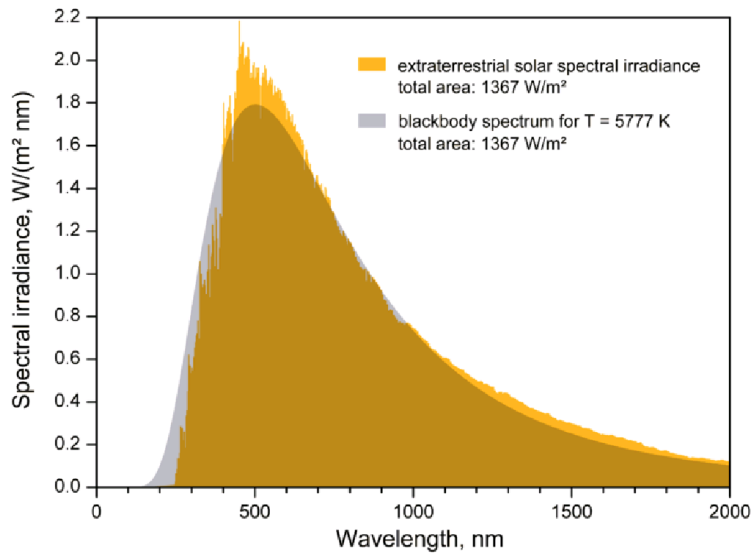


Figure 1.4. Solar spectrum compared with a black body spectrum.

1.2.4 Photosphere

The effective temperature, or black body temperature of the Sun, 5777 K, is the temperature that would have a black body of the same size that radiates the same power.

The photosphere, visible surface of the Sun, is the surface below which the Sun becomes opaque in visible light. Above the photosphere, visible light propagates freely into space and its energy is fully radiated. The change in opacity results from the decrease of H^- ion concentration: these ions are the main absorbers of visible light. Conversely, the light that reaches the Earth is dominantly produced by the interaction of electrons with hydrogen atoms, producing H^- ions. The thickness of the photosphere varies from several tens to several hundreds kilometres, corresponding to an opacity slightly smaller than that of the Earth atmosphere. The Sun light has a spectrum close to that of a black body superimposed on atomic lines radiated from the top of the photosphere. The photosphere has a density of $\sim 10^{23} \text{ particles/m}^3$, namely $\sim 1\%$ of that of Earth at sea level.

1.2.5 Atmosphere



Figure 1.5. Total solar eclipse revealing the corona.

During a total solar eclipse it is possible to see the corona with the naked eye. The parts of the Sun above the photosphere are collectively called solar atmosphere. They are visible at all wavelengths, from radio to gamma rays. They include five main zones: the temperature minimum, the chromosphere, the transition region, the corona and the heliosphere. The latter, the higher solar atmosphere, reaches beyond Pluto's orbit to the heliopause where it forms an abrupt shock front at the border with interstellar matter. Chromosphere, transition region and corona are much hotter than the solar surface. This temperature rise is not well understood but is believed to be associated with Alfvén waves having enough energy to heat up the corona. The coolest layer of the Sun is that of the temperature minimum, some 500 km above the photosphere, with a temperature of some 4 kK, low enough to allow for the presence of some simple molecules such as CO and H₂O that are detected by their absorption lines. Above the minimum temperature layer, the chromosphere is some 2'000 km thick. It displays a characteristic spectrum with a rich set of emission and absorption lines. Its temperature increases progressively with altitude, reaching some 20 kK at the top, where helium is partially ionised.

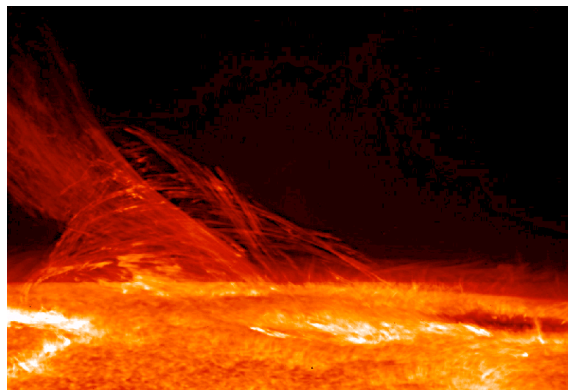


Figure 1.6. Picture was taken by the Hinode's Solar Optical Telescope on January 12th 2007. It reveals the filamentary nature of the plasmas connecting regions of different magnetic polarities.

Above the chromosphere, the transition region is only 200 km thick. Its temperature increases steeply to near the million K in the corona. This increase is due in part to the full ionization of helium in the transition region, significantly reducing the radiative cooling action

of the plasma. The altitude of the transition region is not well defined. It consists in halos embedding turbulences of the chromosphere, spicules or filaments, and is the seat of a constant chaotic motion. It is difficult to observe it from ground, but it can easily be studied from space using detectors sensitive to the far UV.

The corona is the higher part of the solar atmosphere, embedding a volume much larger than that of the Sun as such. It expands into space to generate the solar wind that fills the whole solar system. The lower part of the corona, near the Sun surface, has a density of 10^{15} to 10^{16} particles/m³. The mean temperature of the corona and solar wind is between 1 and 2 MK, reaching 8 to 20 MK in the hottest regions. We lack a theory accounting for the corona temperature but one knows that part of the heat it receives is related to magnetic reconnections.

The heliosphere, which includes the solar wind, covers from some 20 solar radii (0.1 AU) to the extreme limits of the solar system. Its inner boundary is defined as the place where the solar wind flux becomes *superalfvénic* – namely faster than Alfvén waves. Turbulences and other movements that occur beyond this limit cannot act on the corona because the speed of transmission of a signal cannot exceed Alfvén velocity.

1.3 Magnetic field

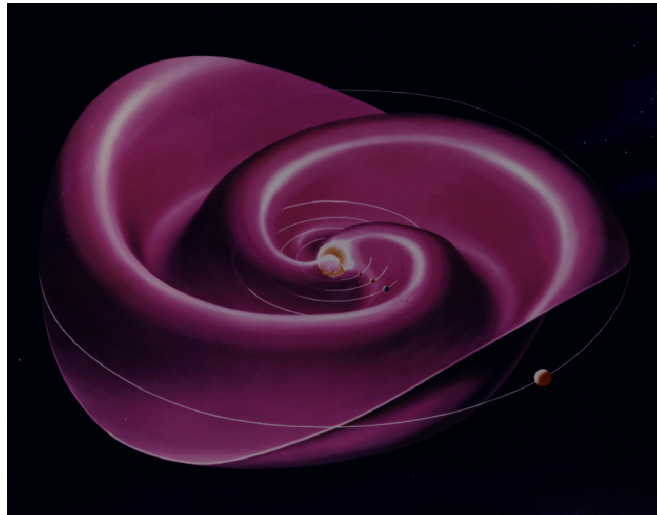


Figure 1.7 Spiral structure of the solar magnetic field.

The solar wind escapes radially in the heliosphere, producing a spiralling magnetic field – because of the solar rotation – that extends to more than 50 AU from the Sun. This rotating magnetic field acts on the currents generated by the plasma motion within the heliosphere.

1.3.1 General features

The Sun is a magnetically active star. It is the seat of a strong and variable magnetic field, that evolves from one year to the next and changes polarity every eleventh year when reaching its maximal activity. This magnetic field is the result of many effects collectively called solar activity. It covers solar spots, fluctuations of the solar wind, flares and major coronal ejections. On Earth, it cause auroras and perturbs electric energy networks as well as radio wave transmission. One thinks that solar activity plaid an important role in the formation and evolution of the Earth via the changes that it induces in the structure of the upper atmosphere.

The dependence of the rotation velocity on latitude causes the dynamo effect by winding field lines that get closer and closer up to producing solar spots and flares before reconnecting and changing polarity. The length of this cycle is about eleven years.

1.3.2 Solar flares

Solar flares were first observed on the Sun by R. C. Carrington and independently by R. Hodgson in 1859 as localized visible brightening of small areas within a sunspot group. A solar flare is a sudden flash of brightness observed over the Sun's surface or the solar limb, which is interpreted as a large energy release of up to $6 \cdot 10^{25}$ J of energy (about a sixth of the total energy output of the Sun each second). They are often, but not always, followed by a colossal coronal mass ejection (CME): the flare ejects clouds of electrons, ions, and atoms through the corona of the Sun into space. These clouds typically reach the Earth a day or two after the event. Solar flares affect all layers of the solar atmosphere (photosphere, chromosphere and corona); the plasma medium is heated to tens of millions of kelvins (several keV, up to MeV scale) and electrons, protons, and heavier ions are accelerated. While an electron having a kinetic energy of 1 MeV has nearly the speed of light, a proton having a kinetic energy of 1 MeV has a momentum of ~ 45 MeV/c, meaning a velocity of $\sim 4.5\%$ of the speed of light. They produce radiation across the electromagnetic spectrum at all wavelengths, from radio waves to gamma rays; most of the energy is spread over frequencies outside the visual range and for this reason the majority of the flares are not visible to the naked eye and must be observed with special instruments. Flares occur in active regions around sunspots, where intense magnetic fields penetrate the photosphere to link the corona to the solar interior. Flares and CMEs are powered by the sudden (timescales of minutes to tens of minutes) release of magnetic energy stored in the corona. Magnetic reconnection occurs when the density of field lines becomes too high. The sudden release of energy in this reconnection is the origin of the particle acceleration. This explains why solar flares typically erupt from what are known as the active regions on the Sun where magnetic fields are much stronger on average. The frequency of occurrence of solar flares varies, from several per day when the Sun is particularly active to less than one every week when the Sun is quiet, following the 11-year cycle.

Flares can affect Earth's ionosphere and disrupt long-range radio communications. They strongly influence the local space weather in the vicinity of the Earth. They can produce streams of highly energetic particles in the solar wind that can impact the Earth's magnetosphere, and present radiation hazards to spacecraft and astronauts. Additionally, CMEs can trigger geomagnetic storms that have been known to disable satellites and knock out terrestrial electric power grids for extended periods of time. Energetic particles in the magnetosphere contribute to auroras.

1.3.3 Interplanetary field

The solar magnetic field extends much farther out than the Sun. The solar wind, a plasma in which the field is anchored, carries magnetic field in the whole solar system, one talks of the interplanetary field. As the plasma moves along the field lines, the interplanetary field is radial near the solar surface. As the magnetic field has different polarities in the northern and southern hemispheres, there exists near the solar equator a thin current layer, the heliospheric current. Away from the Sun, the field lines wind up in an Archimedes spiral, called Parker spiral. The interplanetary field is much stronger than the dipole component of the solar magnetic field. The latter reaches between 50 and 400 μT in the photosphere, and decreases as the distance cubed to reach 0.1 nT at the level of the Earth orbit, where however the interplanetary field is hundred times stronger, reaching some 5nT.

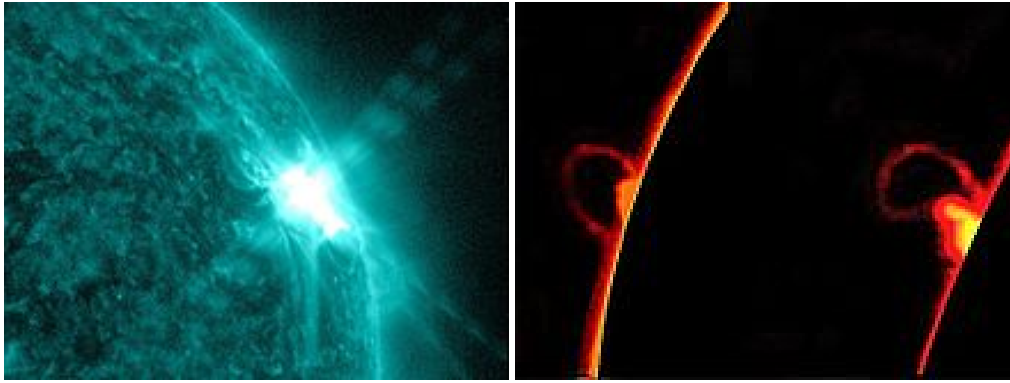


Figure 1.8. Left: An M7.9 class Solar Flare. Right: Two successive photos of a solar flare phenomenon. The solar disc was blocked in these photos for better visualization of the flare's accompanying protruding prominence.

The superposition of the Earth dipole on the interplanetary field produces the Earth magnetosphere. Its structure is complex. In particular the higher density of field lines near the poles trap the solar wind particles to produce auroras.

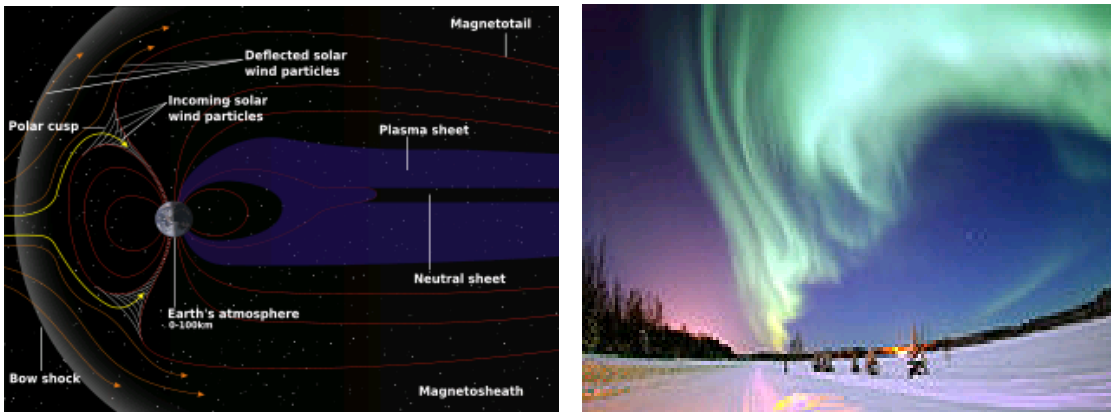


Figure 1.9. Schematic structure of the magnetosphere (left) and picture of an aurora (right).

1.3.4 Solar spots and solar cycle

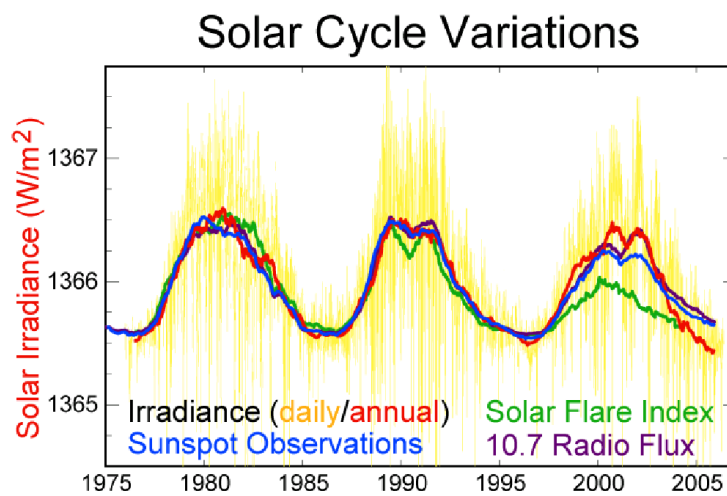


Figure 1.10. The three most recent completed solar cycles.

When one observes the Sun with proper filters, one immediately notices the presence of spots. These are well defined regions that are darker than their surrounding because they are less hot. They are areas of intense magnetic activity preventing convection to take place and therefore reducing the amount of heat transferred from the interior to the surface. The result is a strong heating of the corona, going together with solar eruptions and coronal mass ejections. The larger spots reach thousands of kilometres in diameter.

The number of solar spots follows the eleven years cycle. Typically, at activity minimum, one sees only very few spots, or even none. Then, as activity increases, spots appear first at large latitudes, then closer and closer to the equator (Spörer law). Spots are usually grouped in pairs of opposite magnetic polarities.

1.3.5 Anomalies

The solar cycle has an important impact on climate, the Sun luminosity being related to its magnetic activity. Minima lasting longer than average tend to be associated with higher Earth surface temperatures. During the XVIIth century, the solar cycle paused for several decades and very few spots were observed during what is called the Maunder minimum or small ice period. Europe then experienced very low temperatures. Other similar minima have been revealed by the study of the tree growth circles.

It so happens that the Sun currently shows some anomalies : while the solar wind and the magnetic field that it carries more than doubled during the past century, it now experiences solar spot minima lasting longer than usual. During the past two decades, the speed of the solar wind has decreased by 3%, its temperature by 13% and its density by 20%. Before the recent surge of activity, its magnetic field was twice as weak as 22 years before. The current maximum is lower than those preceding (Figure 1.12). A result is a decrease of the volume of the heliosphere and an increase of the flux of cosmic ray reaching the Earth. Such anomalies are not understood.

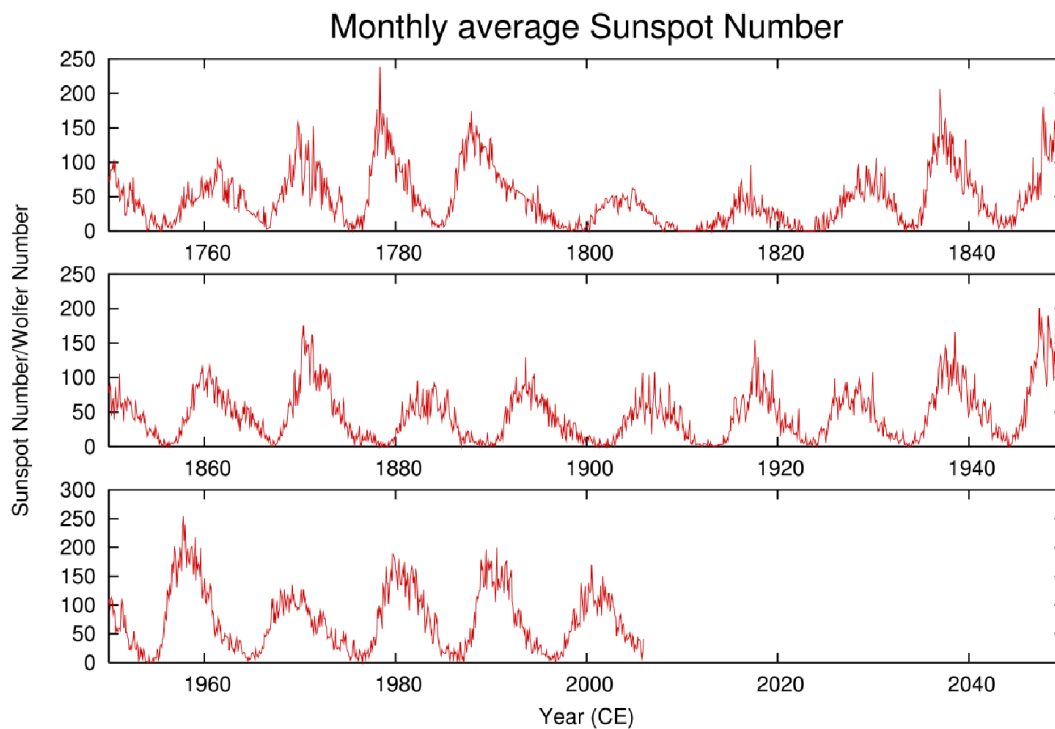


Figure 1.11. Distribution of the observed solar spot number (monthly averages) over the past 250 years.

1.4 Evolution

1.4.1 Birth of the Sun

The Sun was born five billion years ago from the gravitational collapse of an hydrogen molecular cloud. One knows its age either from the general knowledge that we have accumulated on main sequence stars or by radiometric dating of the oldest isotopes of the solar system. Both methods give the same result, 4.57 billion years.

The Sun is essentially made of hydrogen and helium, amounting respectively to 74.8% and 23.7% of the mass inside the photosphere. The heavier elements, collectively called metals by astrophysicists, amount to less than 2% (0.8% of oxygen, 0.3% of carbon, 0.2% of neon and 0.2% of iron).

The Sun inherited these heavier elements from the interstellar matter of which it has been made. Hydrogen and helium are from the nucleosynthesis that followed the Big Bang by some 3 minutes; heavier elements were produced by stellar photosynthesis in the stars which died before the Sun was born. One takes it as granted that the chemical composition of the photosphere is the same as that of the primordial solar system. Yet, since its birth, the Sun has lost helium and heavy elements in its outer layers, which have migrated inward: the photosphere today contains less helium and only 84% of the heavy elements that were contained in the protostellar Sun (71.1% hydrogen, 27.4% helium and 1.5% metals).

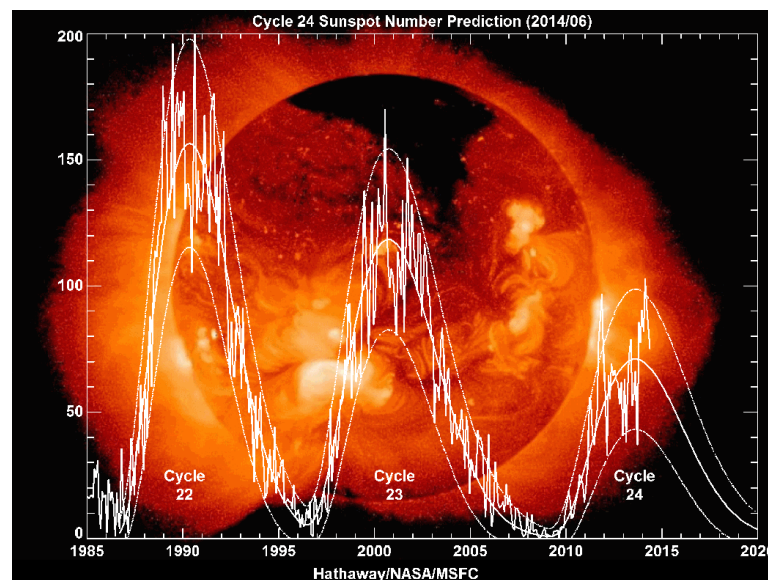


Figure 1.12. Sun spot numbers from 1985 up to now.

1.4.2 Present phase

Available theoretical models that describe the evolution of the Sun tell us that three billion years ago the Sun luminosity was only 75% of the present luminosity. At that time it would then have been impossible to retain liquid water on the surface of the Earth and life could not have appeared as it did. However, geological data show that the Earth remained at more or less a same temperature during its whole history, if anything the young Earth was a bit warmer than it is today. It seems that the reason was a larger concentration of greenhouse gases in the atmosphere (CO_2 , methane, ammoniac) which were keeping the heat to compensate the lesser Sun irradiance.

The Sun is about at the middle of its life, namely of its evolution on the main sequence. Each second, over four million tons of water are turned into energy within the solar core,

producing neutrinos and photons. By now, the Sun already consumed some hundred solar masses. In total, it should spend some ten billion years on the main sequence.

In the Sun interior, nuclear fusion has modified the helium abundance which has now reached 60%. Of course, the metal abundance has not changed. As the Sun interior is radiative rather than convective, none of the fusion products had a chance to migrate outward to the photosphere. An important measure of heavy metal abundance is provided by meteorites, which never reached fusion temperature and are good witnesses of the composition of the protostellar Sun.

1.4.3 Death of the Sun

The Sun is not massive enough to end in a supernova explosion. Some five billion years from now, it will become a red giant, its outer envelope will expand at the same time as its core will contract and warm up (Figure 1.13). Helium will fuse into carbon when the temperature will reach some 100 MK.

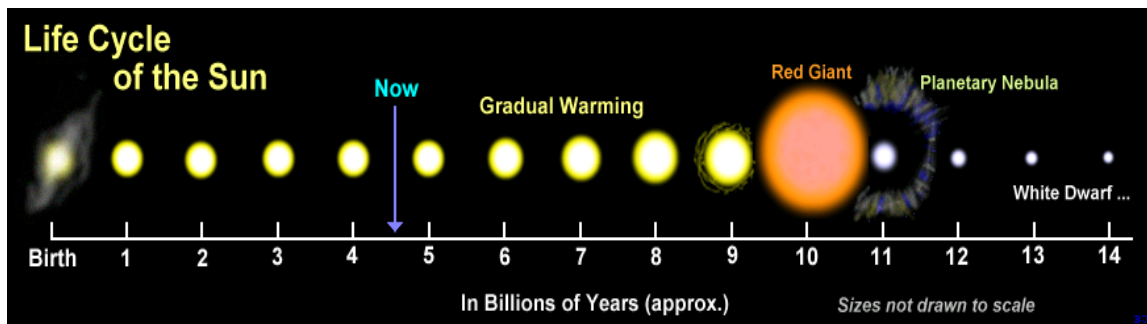


Figure 1.13. Schematic representation of the Sun evolution.

At the end of the red giant phase, large amplitude oscillations will eject the circumsolar envelope that will become a planetary nebula. The core will contract and become a white dwarf which will slowly cool down over billions of years.

2. DATA REDUCTION

The data used in the study had been collected between April 2012 and September 2012 and between October 2013 and January 2014 using the VATLY radio telescope. They were taken by tracking the Sun on-the-flight and have been used to study oscillations that were first reported in Reference [3] before being understood to be caused by multipathing (References [2]). As a byproduct, flares had been identified that had been rejected from the oscillation analysis and which are the sample on which we have worked.

Reports on the performance of the telescope (Figure 2.1 left) are available in Reference [3] and [5]. Frequency spectra are made of three juxtaposed bandwidths covering together ~ 1.08 MHz in 138 bins of ~ 7.8 kHz each; the gain displays a small frequency dependence, $\sim 1.0 \cdot 10^{-4}$ /kHz and a small non linearity reaching 6.2‰ on the Sun. Moreover, the gains of each of the three independent bandwidths fluctuate by 2 to 3‰ with respect to each other and are slightly higher in the centre of each bandwidth than on its edge, by typically 6‰, meaning an average correction of 2.6‰ on the Sun. The beam is well described by a Gaussian having a σ of 2.3° and the pointing accuracy is measured to be 0.22° in *acosh* and 0.11° in *h* where *a* and *h* are the azimuth and elevation respectively

The flare sample included 34 solar flares, 27 of which were detected during the second campaign of observations. The oscillation analysis was performed in parallel with that of data collected simultaneously at the same frequency (1415 MHz) by the Learmonth solar observatory (Figure 2.1 right). Ha Noi and Learmonth are located at nearby longitudes (105.8°E and 114.1°E respectively) and at nearly opposite latitudes (21.0°N and 22.2°S respectively). The technical characteristics of the Learmonth radio telescope are essentially identical to those of the Ha Noi telescope, apart from the use of a linear rather than helical sensor, implying detection of the linear rather than circular component of the wave. The observatory is staffed seven days a week from sunrise to sunset and contributes data to the US Air Force Weather Agency, to the US National Oceanic and Atmospheric Administration and to the Global Oscillation Network Group. In addition to the 2.4 m dish, it operates an 8.5 m dish (245 to 610 MHz), a 1 m dish (15.4 GHz), a swept frequency interferometric radiometer (30 to 80 MHz) and an optical telescope. Its long experience with solar measurements and its commitments to serve a large community make it a highly reliable source of data. The noise level is a factor ~ 1.7 lower for the Learmonth radio telescope than for that in Ha Noi.



Figure 2.1 Left: the Ha Noi antenna. Right: the 2.4 m and 1 m antennas in Learmonth.

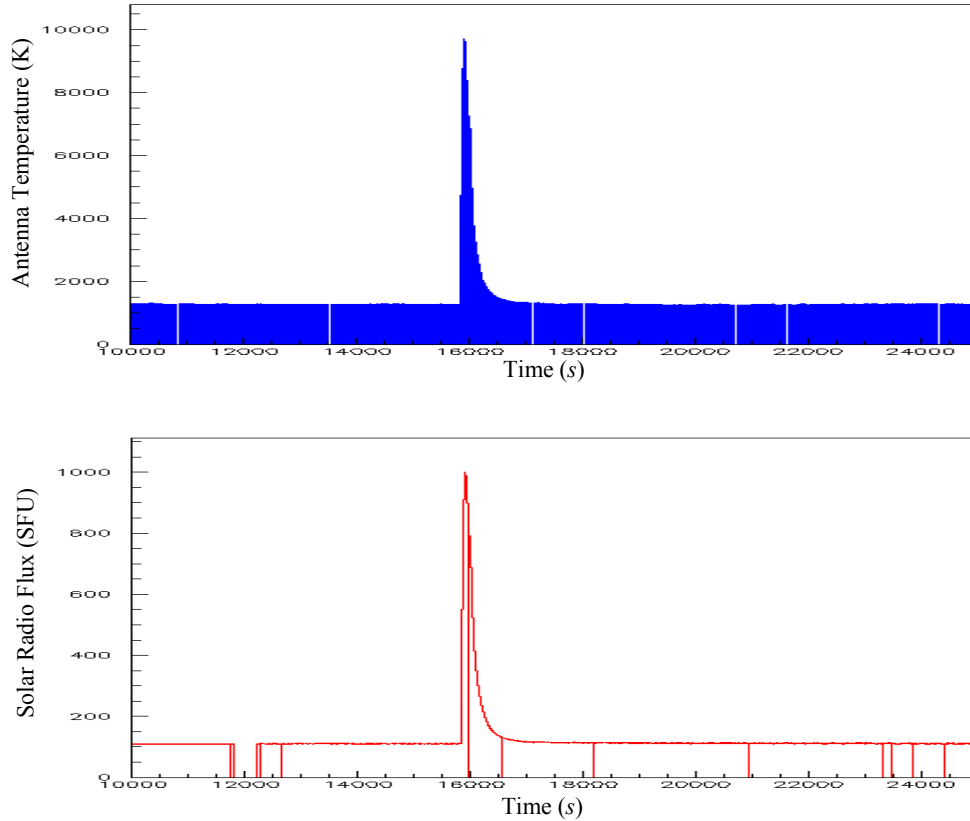


Figure 2.2. A typical flare: raw data for Ha Noi (up) and Learmonth (down). The abscissa is UT time in seconds. In the Learmonth case, there is in principle one measurement at each second. In the Ha Noi case, there is, in principle, one measurement every 8.2 s or so. The resolution of the picture prevents to see the fine structure that results and causes the area below the Ha Noi curve to be fully coloured. In both Learmonth and Ha Noi cases, one notes short periods during which measurements are missing.

The time dependence of the flux emitted by a typical flare is illustrated in Figure 2.2 that displays both the Ha Noi and Learmonth observations. Each measurement is averaged over the bandwidth, of 1.08 MHz. The average is done for us in the Learmonth case, the data being available on the web [1] at 1 second intervals in solar flux units (1 SFU=10⁴ Jy). In the Ha Noi case, they are calculated by us by summing the 138 frequency channels of spectra such as that displayed in Figure 2.3. The Ha Noi data are collected in intervals of ~8.17 s and the measurement is of the antenna temperature. From Reference [5], the conversion factor is 1.25 K/kJy.

In both the Learmonth and Ha Noi data there are time intervals for which measurements are missing. The reason may be the need to recalculate a pointing correction or the presence of a man-caused interference causing a narrow spike, or the transient dysfunction of some electronics component. Moreover, in order to compare Learmonth and Ha Noi data, we decided to use a common time scale in bins of one second. This implied, for each time value (in a sequence of 1 s intervals) to interpolate the Hanoi measurements. The result obtained in the case of the flare illustrated in Figure 2.2 is displayed in Figure 2.4 left.

At that stage, we define by eye two time limits, t_1 and t_2 , bracketing the flare and we use the flux distribution outside these limits to fit a linear background describing the Sun emission before and after the occurrence of the flare. We use it to define the flare flux, S_{flare} , integrated between t_1 and t_2 and background subtracted, and the mean quiet Sun emission during the flare, S_{quiet} , defined as the value taken by the linear background at time $t_{average} = \frac{1}{2}(t_1 + t_2)$. The procedure is illustrated in Figure 2.4 right.

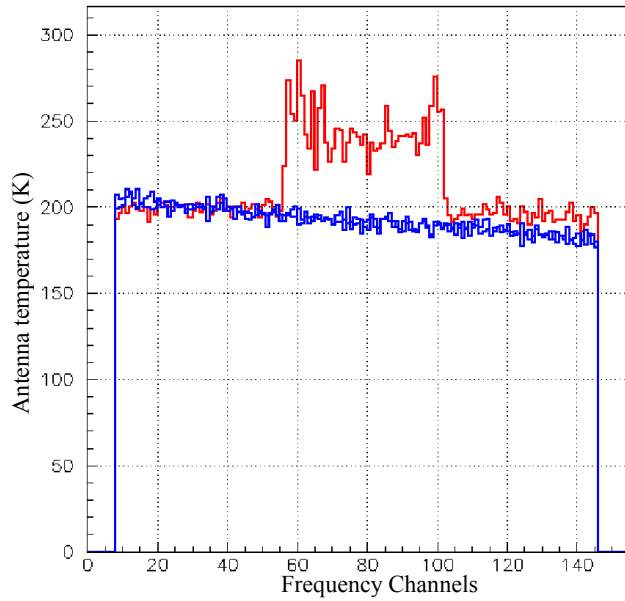


Figure 2.3. A typical frequency spectrum (blue). In some rare cases, as a result of man-caused interferences or of a transient on the power line, a spike occurs in the time distribution of the antenna temperature, associated with a dysfunction of the electronics as shown in red.

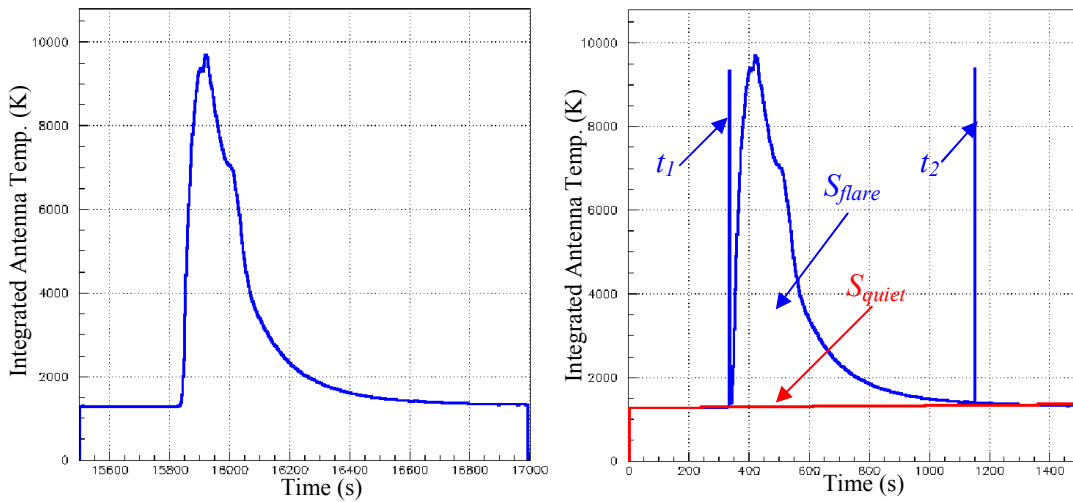


Figure 2.4. Left: the flare displayed in Figure 2.2 (Ha Noi data) after conversion to 1 s bins and interpolation across missing measurements. Right: the same showing the limits t_1 and t_2 and the linear background (red).

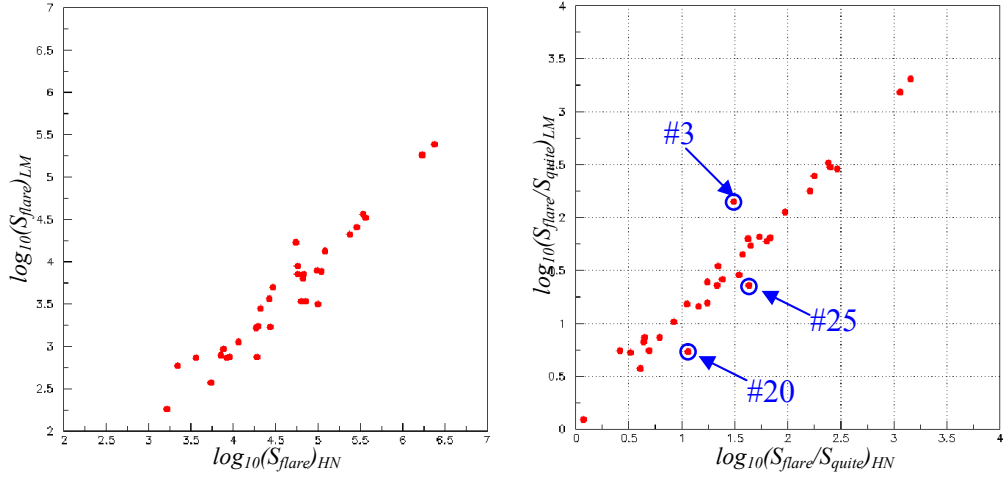


Figure 2.5. Left: scatter plot of S_{flare} in the Learmonth (ordinate) vs Ha Noi (abscissa) plane. The quantities plotted are $\log_{10}(S_{flare})$. Right: Same, with the quantities plotted being $\log_{10}(S_{flare}/S_{quiet})$.

The scatter plot of S_{flare} in the Learmonth/Ha Noi plane is shown in Figure 2.5 left. It shows an important dispersion that is significantly reduced when normalizing S_{flare} to S_{quiet} , showing that much of the dispersion is due to gain drifts rather than different levels of the background sky in Ha Noi and Learmonth. Indeed, a change of gain affects S_{flare} and S_{quiet} , in the same way and leaves their ratio invariant, while a change in sky background level affects only S_{quiet} .

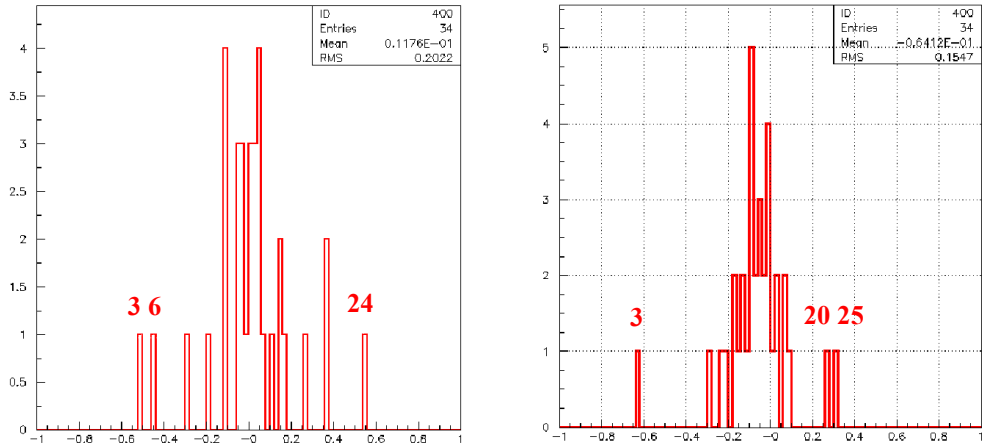


Figure 2.6. Left: distribution of $\log_{10}(0.1 S_{flare, Ha\ Noi} / S_{flare\ Learmonth})$. Right: same distribution with the values of S_{flare} normalized to S_{quiet} .

This is made more visible in Figure 2.6 left by plotting the distribution of $\log_{10}(0.1 S_{flare, Ha\ Noi} / S_{flare\ Learmonth})$. We expect its mean value to be $\log_{10}(1.25) = 0.01$, which it is. The same distribution with the values of S_{flare} normalized to S_{quiet} is displayed in Figure 2.6 right.

The last step consists in normalizing the flux distributions to a common flux scale by dividing the measured fluxes by the associated values of S_{flare} . The result is displayed in Figure 2.7 for the flare of Figure 2.2. It is then possible to define a χ^2 measuring the quality of the agreement between the Ha Noi and Learmonth measurements. However, before doing so, we optimize the time delay Δt to be applied to the Ha Noi data with respect to the Learmonth data by minimizing the associated value of χ^2 . We expect the best fit value of Δt to cancel within

$\sim \pm 4$ s. Its mean value is 1.8 s and the rms 3.9 s. The results are listed in Table 2.1 for each of the 34 flares. The distributions of Δt and χ^2 are displayed in Figure 2.8. The distribution is very broad, it is studied in the next chapter.

Table 2.1 Parameters of the 34 selected flares

Nr	Date	S_{flare}		S_{quiet}		Δt (s)	$\log_{10}(\chi^2)$
		Learmonth (SFU)	Ha Noi (K)	Learmonth (SFU)	Ha Noi (K)		
1	131025_01	6'412	64'183	115.8	1407	4	-6.8
2	131025_02	244'673	2'364'007	117.9	1511	-4	-6.8
3	131025_03	16'258	50'527	117.9	1534	3	-6.1
4	131026_01	7'414	106'625	114.8	1610	2	-6.3
5	131028_01	35'868	342'326	116.1	1358	4	-6.8
6	131029_01	607	2'181	112.2	778	2	-4.3
7	131102_01	1'129	12'199	111.0	1501	3	-4.9
8	131103_01	394	5'573	107.0	1307	6	-4.4
9	131105_01	1'737	18'020	109.6	1404	1	-3.9
10	131106_01	1'764	26'271	114.1	1449	5	-5.3
11	131106_02	764	6'814	109.8	1434	4	-4.8
12	131107_01	20'851	234'031	109.7	1308	2	-5.9
13	131108_01	764	8'740	109.9	1305	3	-4.1
14	131108_02	188'217	1'685'342	115.4	1315	1	-6.4
15	131110_01	25'713	285'390	110.4	1382	2	-5.7
16	131112_01	7'743	98'392	125.8	1519	4	-6.1
17	131113_01	1'643	18'717	120.4	1397	2	-5.8
18	131117_01	184	1'736	142.4	1627	6	-3.0
19	131118_01	754	8'983	139.6	1541	5	-4.5
20	131118_02	765	18'128	134.4	1566	-2	-5.5
21	131207_01	34'955	378'063	123.5	1465	-1	-7.4
22	131212_01	3'643	28'075	148.0	1554	5	-6.5
23	131215_01	721	3'724	130.0	1117	2	-4.3
24	140101_01	2'957	105'192	111.1	4277	2	-5.8
25	140108_01	3'217	76'725	143.2	1822	-1	-5.9
26	140110_01	896	7'894	132.8	1731	2	-5.4
27	131117_02	6'662	69'209	143.7	1738	5	-6.4
28	120427_01	7'943	60'493	121.8	1083	0	-6.8
29	120507_01	2'628	20'215	122.8	953	-2	-4.9
30	120703_01	34'307	363'510	116.4	1254	4	-4.9
31	120706_01	12'797	121'356	116.4	1231	-1	-5.3
32	120709_01	4'758	30'375	133.4	1377	-7	-5.5
33	120710_01	8'073	63'009	139.5	1571	-13	-4.6
34	120904_01	3'376	62'383	122.2	1866	0	-5.5

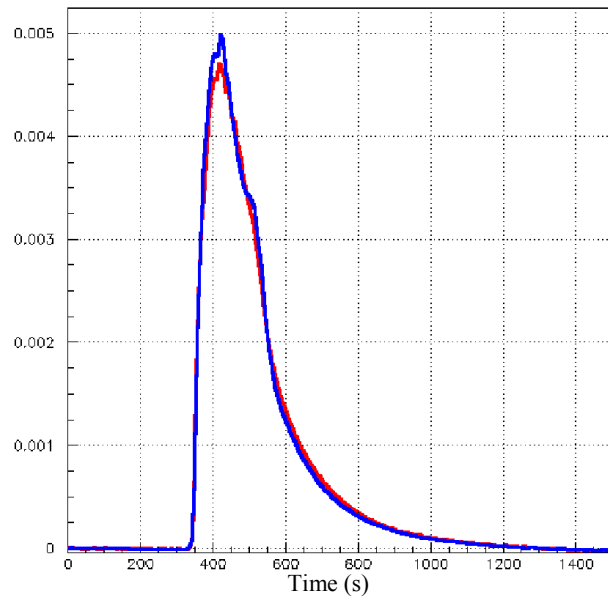


Figure 2.7. The flare of Figure 2.2 after normalisation to unit area between t_1 and t_2 . Ha Noi data are shown in blue and Learmonth data in red.

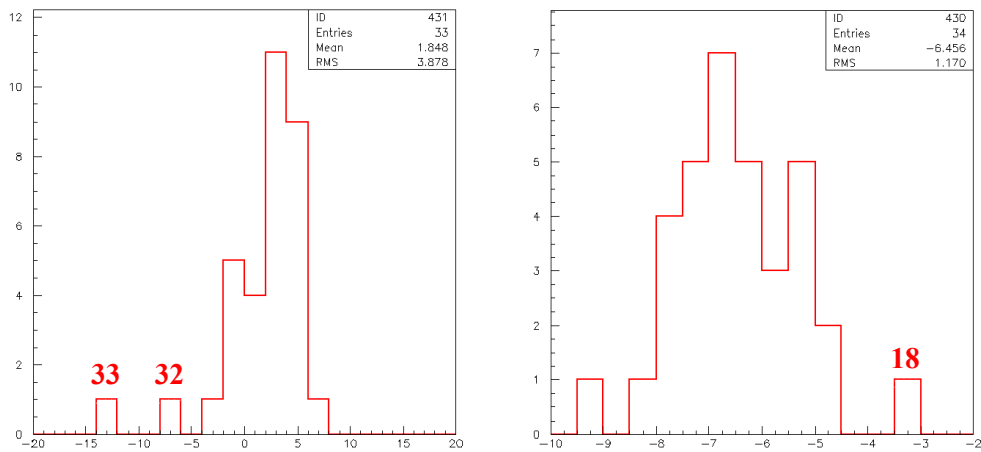


Figure 2.8. Left: distribution of the best Δt values. Right: distribution of the best values of $\log_{10}(\chi^2)$ where χ^2 has been divided by the width of the flare interval, $t_2 - t_1$.

3. DETAILED STUDY OF THE SELECTED FLARES

The six largest flares, defined as having integrated fluxes exceeding 20'000 SFU in the Learmonth data and integrated antenna temperatures exceeding 200'000 K in the Ha Noi data, have been retained for further analysis.

3.1 Learmonth-Ha Noi comparison at 1.4 GHz

The data from Table 2.1 are repeated below and the flares are renamed as 1 to 6. The mean value of Δt is 1 s with an rms of 3 s. The Learmonth and Ha Noi profiles are displayed in Figure 3.1.

Table 3.1 Parameters of the six larger flares retained in the study

<i>Nr</i>	<i>New Nr</i>	<i>Date</i>	<i>S_{flare}</i>		<i>S_{quiet}</i>		<i>Δt (s)</i>	χ^2 (10^{-7})
			<i>Learmonth (SFU)</i>	<i>Ha Noi (K)</i>	<i>Learmonth (SFU)</i>	<i>Ha Noi (K)</i>		
2	1	131025-02	244'673	2'364'007	117.9	1511	-4	2
5	2	131028-01	35'868	342'326	116.1	1358	4	2
14	3	131108-02	188'217	1'685'342	115.4	1315	1	4
15	4	131110-01	25'713	285'390	110.4	1382	2	20
21	5	131207-01	34'955	378'063	123.5	1465	-1	4
30	6	120703-01	34'307	363'510	116.4	1254	4	126

The agreement between the Ha Noi and Learmonth profiles is generally good. However, we note differences in the highest flux regions, which we now study.

Zooms on the peaks of flares 1 and 2, displayed in Figure 3.2, reveal two causes of disagreement between the Ha Noi and Learmonth data. First, as clearly evidenced in the case of flare #1, the Ha Noi electronics fails to record very high or very rapidly changing signals. Second, the signals are averaged over longer integration times in Ha Noi than in Learmonth, 8 s instead of 1 s, precluding the observation of fine structures as can be seen from flare #2 in Figure 3.2. While the latter is trivial, the former deserves a closer look.

Figure 3.3 displays successive frequency spectra recorded over the peak of flare #1. As the flux increases, one first sees changes in slope and differentiation between the three bandwidths stitched together to form the spectrum, followed by a complete failure of the system as in measurements 12 to 14. Such dysfunctions are known to occur and have already been mentioned in Reference [5]. After such dysfunction, the system is seen to recover rapidly: measurement 20 and following display a normal behaviour.

3.2 Learmonth radio data at different frequencies

Flares 1 to 6 have been observed in Learmonth at eight different frequencies (245 MHz, 410 MHz, 610 MHz, 1415 MHz, 2695 MHz, 4995 MHz, 8800 MHz and 15400 MHz). Figure 3.4 displays their profiles in log scale, showing that they are present at all frequencies.

Figures 3.5 and 3.6 show the frequency dependence of the profiles of the two larger flares, 1 and 3. Low frequencies display very high and narrow early spikes while higher frequencies display slowly decreasing tails. We had no time to correlate such frequency dependence with the different physics mechanisms responsible for the energy release.

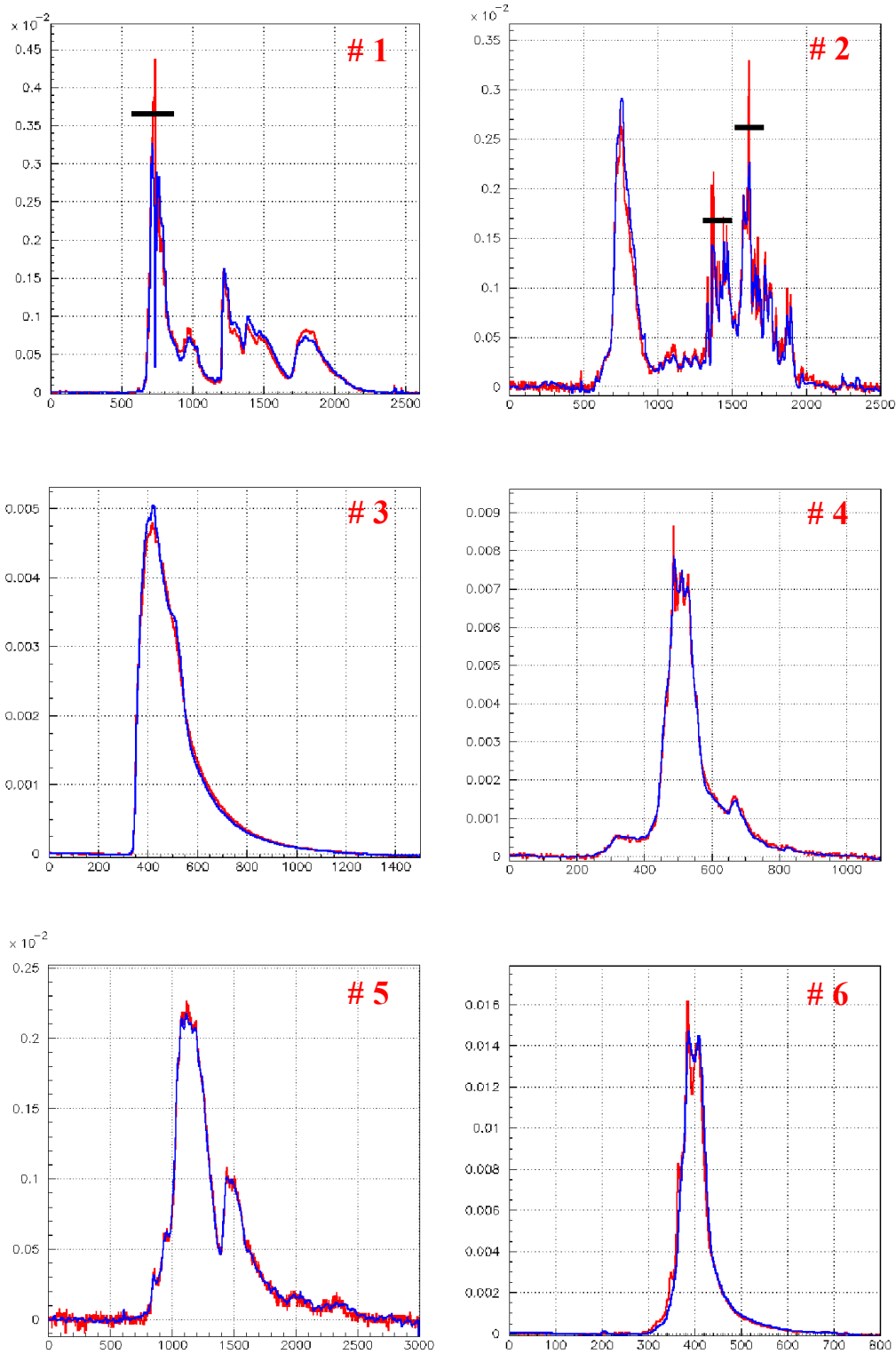


Figure 3.1. Learmonth (red) and Ha Noi (blue) profiles of the selected flares. The thick bars indicate the peak regions displayed in Figure 3.2.

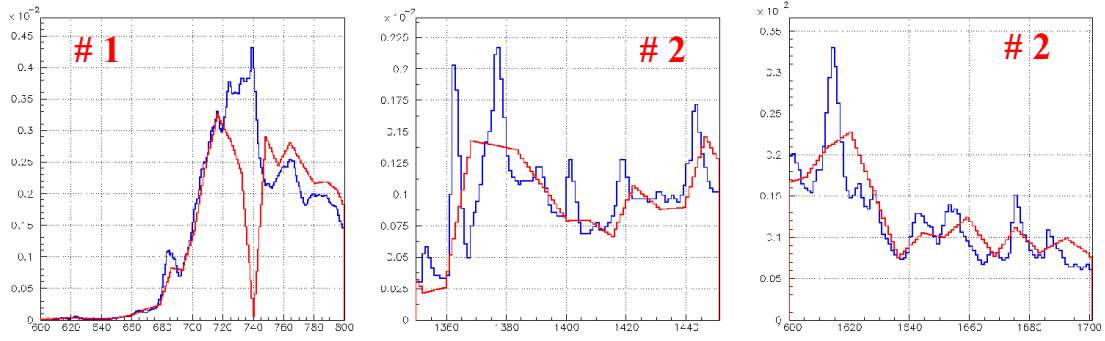


Figure 3.2. Zoomed profiles on the peaks of flares 1 and 2 as indicated in Figure 3.1.

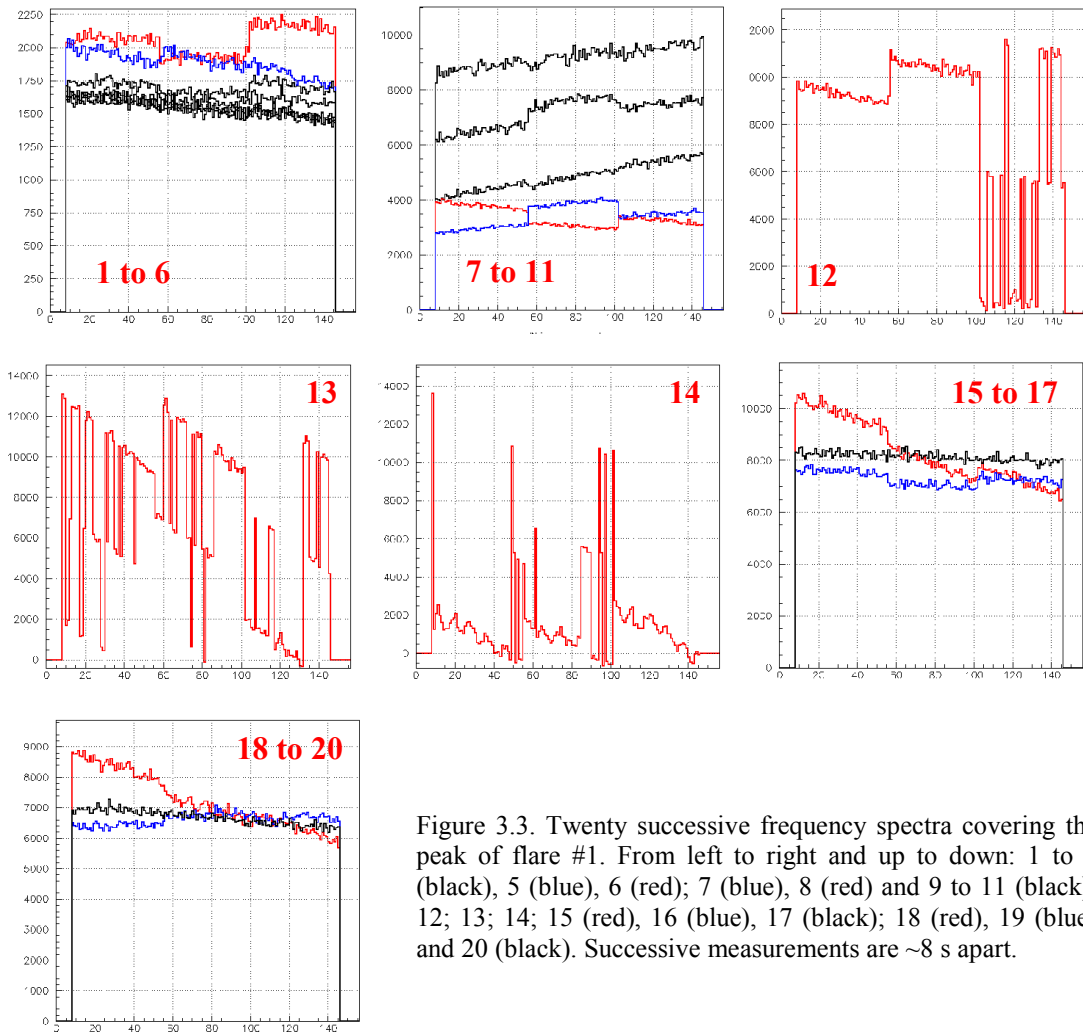


Figure 3.3. Twenty successive frequency spectra covering the peak of flare #1. From left to right and up to down: 1 to 4 (black), 5 (blue), 6 (red); 7 (blue), 8 (red) and 9 to 11 (black); 12; 13; 14; 15 (red), 16 (blue), 17 (black); 18 (red), 19 (blue) and 20 (black). Successive measurements are ~ 8 s apart.

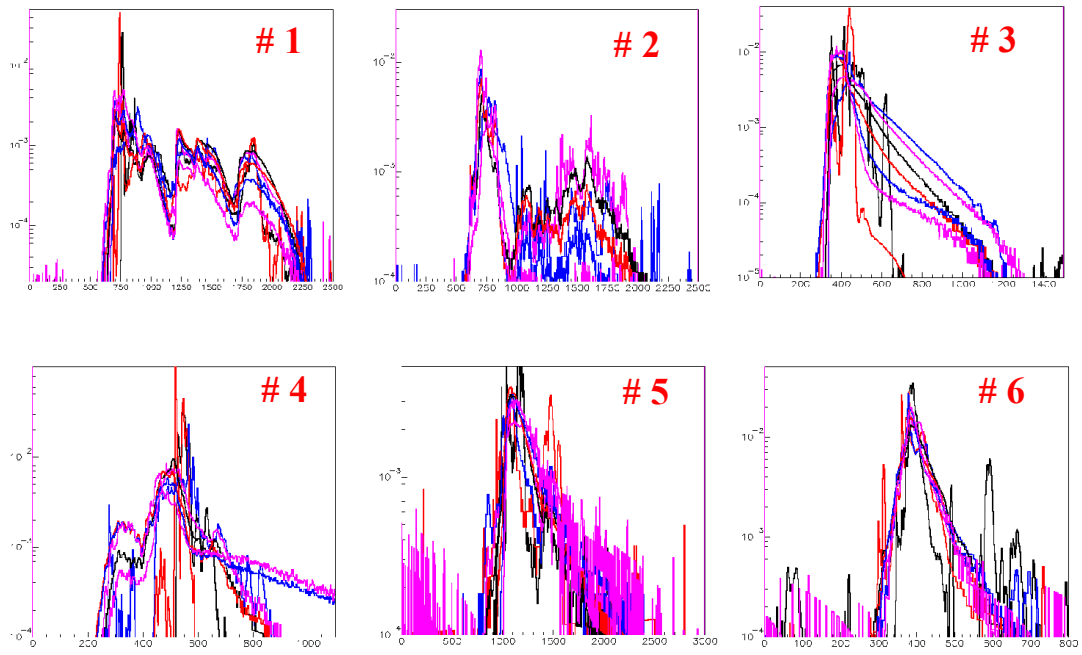


Figure 3.4. Flares at different frequencies in Learmonth: 245 MHz (black), 410 MHz (red), 610 MHz (blue), 1415 MHz (purple), 2695 MHz (black), 4995 MHz (red), 8800 MHz (blue) and 15400 MHz (purple).

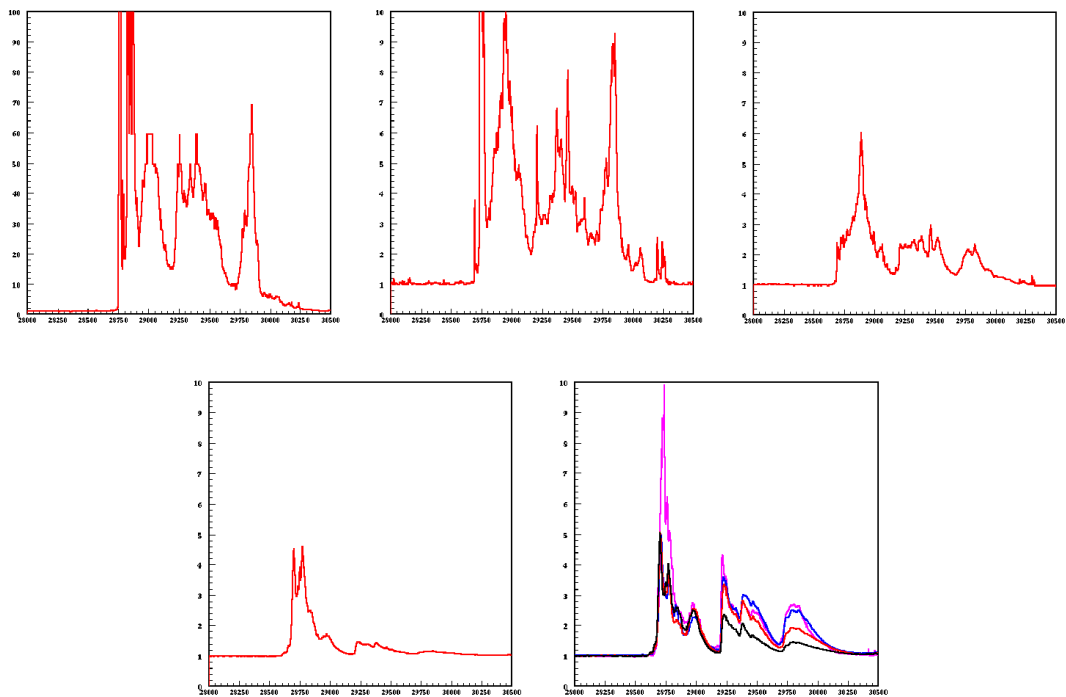


Figure 3.5. Flare #1 profiles. Up left, 245 MHz, peaks at 1550; up middle, 410 MHz, peaks at 285; up right, 610 MHz; down left, 1415 MHz; down right: 2695 (magenta), 4995 (blue), 8800 (red) and 15400 (black) MHz .

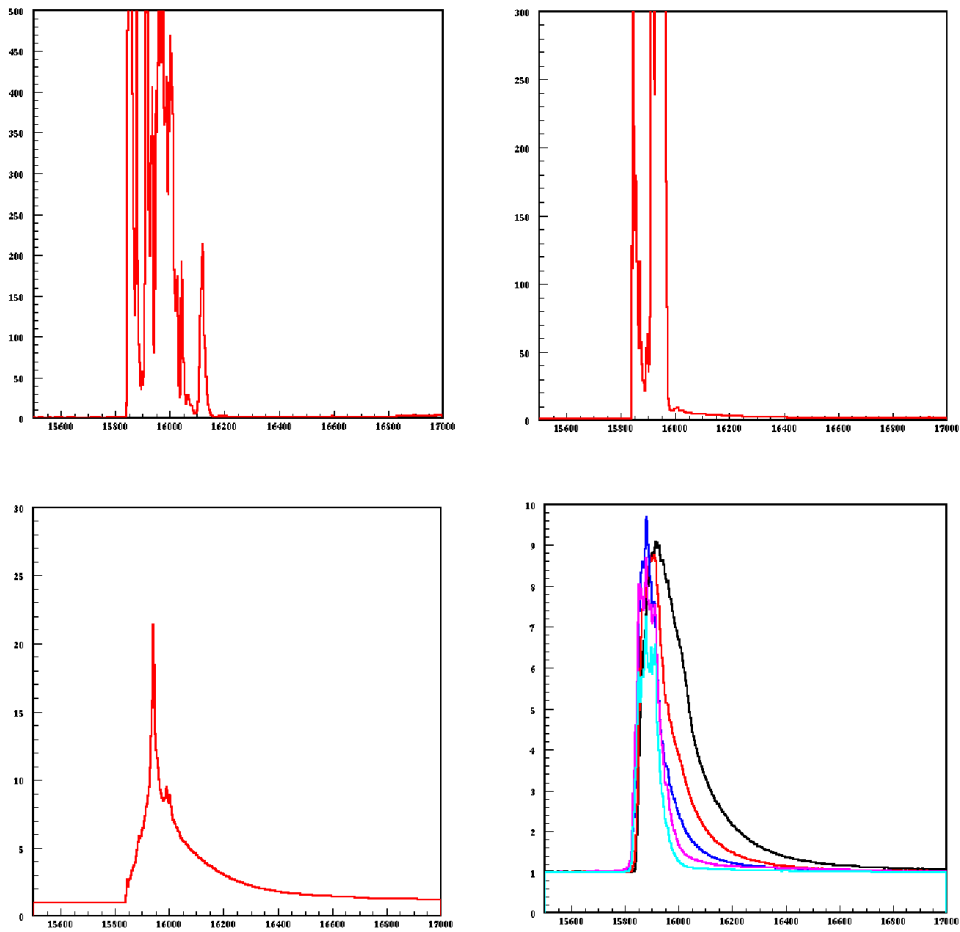


Figure 3.6. Flare #3 profiles. Up left, 245 MHz, peaks at 1670; up right, 410 MHz, peaks at 3050; down left, 610 MHz; down right, 1415 MHz (black), 2695 (red), 4995 (blue), 8800 (magenta) and 15400 (cyan) MHz.

3.3 Other wavelengths

X-ray data were downloaded from the website of the Japan Aerospace Exploration Agency [6]. These data were collected by the GOES-15 satellite, which is part of the US National Oceanic and Atmospheric Administration (NOAA) Geostationary Operational Environmental Satellite (GOES) system. X-ray data are recorded every minute. The X-ray wavelength is in the 0.1 nm to 0.8 nm range. The six X-ray profiles are compared with the 1415 MHz radio profiles in Figure 3.7, normalized to a same quiet Sun level and interpolated from minute to second. Relative to quiet Sun, X-ray flares are much larger than radio flares. They are seen to precede the radio flares by typically one to two minutes. Information concerning the location of the flares, available from the web [8], is listed in Table 3.2. Note that flare #4, which is classified as an X flare, seems to peak at only half the levels of flares #1 and #3 in Figure 3.7. The reason is that the quiet Sun is at twice as low a level for flare #4 than for the two other flares. The classification of flares is such that M flares are a factor 10 below X flares and within each category the index corresponds to a log scale divided in 10 intervals. When plotted in absolute fluxes, the data check well with the classification listed in Table 3.2 below.

Extreme ultraviolet (EUV) data obtained by GOES-14 at one minute intervals with wavelengths in the 5 nm to 15 nm range are downloaded from the web (Laboratory for Atmospheric and Space Physics) [7] and displayed in Figure 3.7. They correspond to much weaker disturbances of the quiet Sun level than radio and X-ray flares do. Again, understanding

the physics phenomena responsible for this frequency dependence would have required more time than was available for the present internship.

Table 3.2 Information on the six X-ray flares and comparison with the 1415 MHz data.

Nr	Date	Flare of Class	Active region	Begin, UT		End, UT		Sunspot coordinate
				X-ray	1415 MHz	X-ray	1415 MHz	
1	131025-02	X1.7	1882	07:56	07:57	08:53	08:28	S22 E37
2	131028-01	M5.1	1875	04:34	04:35	05:50	05:01	N07 W64
3	131108-02	X1.1	1890	04:23	04:24	04:43	04:38	S11 E10
4	131110-01	X1.1	1890	05:08	05:09	05:33	05:20	S11 W15
5	131207-01	M1.2	1909	07:17	07:18	09:10	07:47	S17 W50
6	120703-01	C9.0	1515	03:36	03:38	04:02	03:43	S17 E04

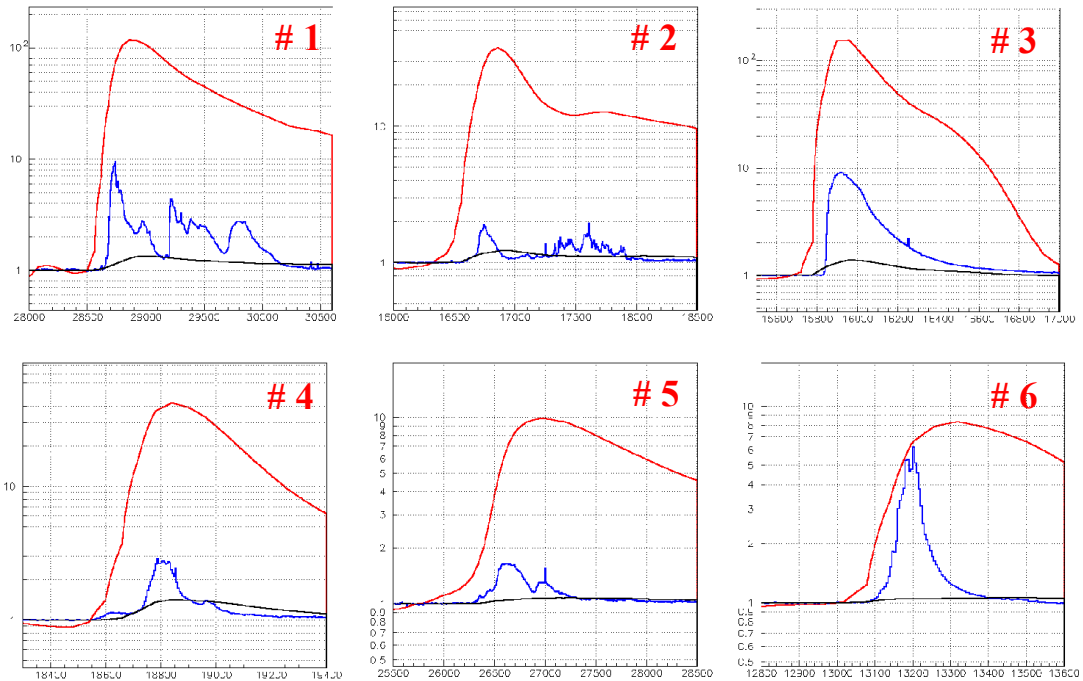


Figure 3.7 Comparison of the X-ray (red), 1415 MHz (blue) and EUV (black) profiles.

4. CONCLUSION

We have examined a sample of 34 solar flares collected using the VATLY radio telescope at 1415 MHz frequency and we have selected the six stronger of them, which we have compared with measurements made in Australia by the Learmonth solar observatory and by satellites in the X-ray and EUV regions. The Ha Noi sample displays a good agreement with the Learmonth sample at the same frequency, except for known dysfunctions of the Ha Noi electronics in the response to particularly large signals. Flare profiles are seen to be strongly dependent on frequency in the radio range, low frequencies displaying short and intense early spikes, high frequencies displaying long decay tails. Compared with the quiet Sun, the X-ray signals are much stronger and the EUV signals much weaker than the radio signals. The X-ray signals tend to start significantly earlier than the others, suggesting a precocious heating of the atmospheric plasma before triggering the magnetic reconnection proper. While roughly simultaneous, the three types of signals, radio, X-ray and EUV, display very different features.

ACKNOWLEDGEMENTS

I would like to express my deep appreciation and thanks to my supervisor Prof. Pierre Darriulat for his patient guidance, advices and inspired me to complete this report.

I am very indebted to Dr. Nguyen Thi Thao who helped me on analysing data, for her valuable suggestions and encouragement during this internship.

I especially thank Nguyen Thi Phuong who helped me in preparing data and making useful comments. I am very grateful to Dr. Pham Ngoc Diep, Pham Tuan Anh and other VATLY staffs. They were very nice, warmly welcome and helped me a lot during this internship. In addition, I would like to thank my classmates, especially Thanh who worked with me for part of the report.

Finally, I would like to thank the University of Science and Technology of Ha Noi, the Vietnam Astrophysics Training Laboratory and the Institute for Nuclear Science and Technology which facilitated our internship.

REFERENCES

- [1]. Australian Government, Bureau of Meteorology, Radio and Space Weather Services, http://www.ips.gov.au/World_Data_Centre/1/10
- [2]. P. N. Diep et al. (2014), *Correlated oscillations due to similar multi-path effects seen in two widely separated radio tetescopes*, PASA, Vol. 31, e029
- [3]. N.V. Hiep et al. (2014), *The VATLY radio telescope*, Comm. Phys., Vol. 22, No. 4, pp. 365-374
- [4]. N.V. Hiep et al. (2014), *Solar Observation of Solar-Activity-Related mHz Oscillations*, Solar Physics, Vol. 289, 3, 939
- [5]. N.T. Phuong et al., 2014, *The VATLY radio telescope: performance study*, accepted for publication in Comm. Phys. Viet Nam
- [6]. Japan Aerospace Exploration Agency, <http://darts.isas.jaxa.jp/pub/solar/mirror/sswdb/goes/xray>
- [7]. Laboratory for Atmospheric and Space Physics, University of Colorado Boulder, http://lasp.colorado.edu/eve/data_access/service/plot_averages/index.html
- [8]. Laboratory of X-ray astronomy of the Sun, http://www.thesis.lebedev.ru/en/sun_flares.html



UNIVERSITE DES SCIENCES ET DES TECHNOLOGIES DE
HANOI

UNIVERSITY OF SCIENCE & TECHNOLOGY OF HANOI

TRƯỜNG ĐẠI HỌC KHOA HỌC & CÔNG NGHỆ HÀ NỘI

**REVIEW ON INTERNSHIP RESULT
MASTER IN SPACE & APPLICATIONS**

STUDENT INFORMATION

Full name : Bui Van Tuan Gender : Male
Date of Birth : 05/03/1990 Email : greenstar5390@gmail.com
Tel : 0979.854.006

RECEPTION INFORMATION

Company/ Organization name: VATLY/ INST
Address : 179 Hoang Quoc Viet, Cau Giay, Hanoi
Supervisor Name : Pierre Darriulat Gender : Male
Tel : 04.37.910.017 Email : darriulat@vinatom.gov.vn
Title : Professor
Department : Centre of Nuclear Physics

REVIEW ON INTERNSHIP RESULT

1. Internship report

The report studies a sample of thirty-four solar flares detected in Hanoi using the VATLY radio telescope at 1.415 GHz between 2012 and 2014. It compares the six largest of them with measurements made at either the same or different frequencies at the Learmonth solar observatory (Australia) and using satellites in the X-ray and EUV regions. The Hanoi data display good agreement with Learmonth data at the same frequency. Flare profiles are seen to be strongly dependent on frequency in the radio range, low frequencies displaying short and intense early spikes, high frequencies displaying long decay tails. Compared with the quiet Sun, the X-ray signals are much stronger and the EUV signals much weaker than the radio signals. The X-ray signals tend to start significantly earlier than the others, suggesting a precocious heating of the atmospheric plasma before triggering the magnetic reconnection proper. While roughly simultaneous, the three types of signals, radio, X-ray and EUV, display very different features.

The work made by the student was shared between purely bibliographic studies and data analysis. The former include textbook studies of solar physics and solar flares as well as a search for data available on the web at X-ray and EUV frequencies. The latter implies simple data analysis including correction for anomalies, interpolation, subtraction of quiet sun contribution, simple χ^2 minimizations, histogramming, etc...

2. Student's qualification

The student has shown a good overall understanding of the study; he was quick in acquiring new knowledge. His bases in physics and informatics were at a level that made it easy for him to catch quickly what he had to learn

3. Student's motivation

The student displayed a keen interest and motivation for his work. He proved to be able to work hard and independently once general guidelines had been given. He displayed a very serious and responsible attitude toward his work

GENERAL REVIEW (Achievement level to Internship of the student)

The performance of the student was excellent and above what could be expected to be achieved in such a short time

Certified by organization of internship
(signed and tamped)

Hanoi,/...../2014
Supervisor (signature)